Time–Frequency Characteristics Research of Common Mode Current in PWM Motor System

Shiran Cao, Feng Niu, *Member, IEEE*, Xiaoyan Huang, *Member, IEEE*, Shaopo Huang, Yao Wang, *Member, IEEE*, Kui Li, and Youtong Fang, *Senior Member, IEEE*

***Abstract*—With the increasing of switching frequency in pulsewidth modulated motor system, common mode current (CMC) seriously affects the reliable operation of motor system and it has become a problem that cannot be ignored. This paper proposes a mathematical model of CMC and conducts detailed time–frequency characteristics analysis of CMC. The influence of several key parameters of motor system, such as distributed capacitance, dc bus voltage, and inverter switching frequency, on CMC characteristics has been analyzed in detail, and the corresponding variation rule of CMC oscillation amplitude and attenuation period/time has been summarized. The experimental results are presented to verify the correctness of theoretical analysis. The conclusions of this paper can lay theoretical foundation for the effective suppression of CMC in various practical applications.**

***Index Terms*—Common mode current (CMC), inverter, pulsewidth modulated (PWM) motor system, time–frequency characteristics.**

I. Introduction

IN RECENT years, the switching performance of power devices has been significantly improved, and correspondingly, the switching frequency of power inverter in pulsewidth modulated (PWM) motor system becomes higher and higher. As a result, the electromagnetic interference (EMI) problem in PWM motor system becomes more and more obvious, which seriously affects the normal operation of motor system and surrounding equipment.

EMI in PWM motor system is mainly composed of two parts: Common mode (CM) current (CMC), also called conducted EMI, and electromagnetic radiation (EMR). CMC is mainly caused by the large du/dt of common mode voltage (CMV) during inverter switching transition which can charge and discharge the distributed capacitance in motor system. The CMC has long been known to cause a variety of problems which include electromagnetic compatibility, bearing currents, and so on.

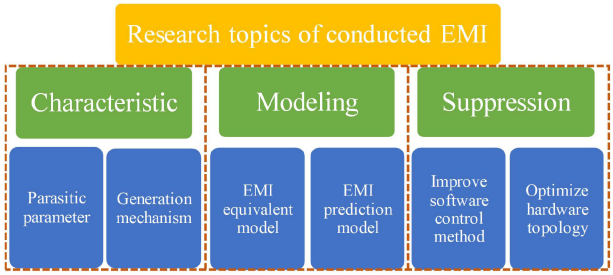

Fig. 1. Research topics of conducted EMI.

In order to effectively understand and suppress EMI, lots of research work have been conducted in related aspects as shown in Fig. 1. EMI characteristic research includes EMI generation mechanism and time–frequency characteristics, EMI modeling research focuses on the equivalent model and prediction model, and EMI suppression research can be divided into control method improvement and hardware topology optimization.

For EMI characteristic research, Lu *et al.* propose a high-frequency model of unshielded four-wire power cable to prove that CMC is related to the cable length, while the skin and proximity effects as well as dielectric losses of cable are taken into consideration in this model [1]. Sunitha *et al.* found that the motor impedance varies with motor power, so the motor systems with same cable length have different line voltage and CMV when the motor power is different [2]. The simplified inverter model proposed in [3] demonstrates that dc bus voltage, switching frequency, and load can influence the amplitude and frequency of EMI. Lai *et al.* found the EMI frequency range related to PWM frequency, device switching, and propagation path when inverter takes MOSFET as switching device [4]. Wang *et al.* has theoretically analyzed the effects of grounding parasitic paths on the performance of CM filter, thereinto, the influence on CM capacitor is most obvious [5]. In addition, Gubia *et al.* propose a frequency-domain-based model which can accurately simulate the behavior of CMC at any point of motor system and allow user to understand the influence of

Manuscript received September 14, 2018; revised December 24, 2018, January 26, 2019, and April 12, 2019; accepted May 6, 2019. Date of publication May 12, 2019; date of current version November 12, 2019. This work was supported in part by the National Natural Science Foundation of China under Grant 51707174, and in part by the Innovative Funding Project for Postgraduate of Hebei Province under Grant CXZZSS2018030. Recommended for publication by Associate Editor M. Trzynadlowski. *(Corresponding author: Feng Niu.)*

S. Cao, F. Niu, S. Huang, Y. Wang, and K. Li are with the State Key Laboratory of Reliability and Intelligence of Electrical Equipment and Hebei Key Laboratory of Electromagnetic Field and Electrical Apparatus Reliability, Hebei University of Technology, Tianjin 300130, China (e-mail: csran@qq.com; niu.feng.hebut@gmail.com; shaopo0303@163.com; wangyao@hebut.edu.cn; likui@hebut.edu.cn).

X. Huang and Y. Fang are with the College of Electrical Engineering, Zhejiang University, Hangzhou 310027, China (e-mail: xiaoyanhuang@zju.edu.cn; youtong@zju.edu.cn).

Color versions of one or more of the figures in this paper are available online at http://ieeexplore.ieee.org.

Digital Object Identifier 10.1109/TPEL.2019.2916686

each system parameter on the CMC [6]. Ogasawara and Akagi think that the CMC flowing path can be expressed as an *RLC* series circuit which can clearly show the effect of system components on CMC time domain waveform [7]. Shen *et al.* proposed that the EMI dominant factors in different frequency ranges are different. For example, the modulation method is dominant factor in low-frequency range (150 kHz–5 MHz), and in high-frequency range (5–30 MHz), the difference of CM loop impedance makes the high-frequency EMI different. Meanwhile, the hardware topology of system also determines the EMI intensity [8]. Since the source of CMC is the CMV, Lian *et al.* found that the third-order component in CMV generated by current-source inverter is influenced by the modulation index in low speed range and the application of PFC may amplify the CMV so as to aggravate CM resonance problem [9]. EMI characteristic research is inseparable from the extraction of system parameters. So, Sun and Xing proposes a parameterization method for multistage linear *RLC* circuits, which can accurately obtain the parameters of each *RLC* stage in a noniterative manner [10].

For the modeling of conducted EMI, Magdun and Binder establish a high-frequency equivalent motor model to simplify the simulation process of conducted EMI [11]. Jiang, Ran *et al.*, and Revol *et al.* propose several analysis and prediction models of conducted EMI which are quite accurate in their corresponding effective bands [12]–[14]. For the suppression of conducted EMI, the related research works mainly focus on the optimization of software control strategy and hardware topology [15]–[17]. For example, Mutoh and Ogata propose two methods to suppress CMC. One is to control differential mode (DM) noises by a special hardware structure, which can split CM noise into ground while eliminating DM noise. Another one is to insert a damping impedance circuit between motor and ground, and this method can prevent series resonance phenomena of CMC [18]. In addition, some scholars have studied the characteristics and modeling of EMR [19]–[21].

In this paper, the time-domain and frequency-domain characteristics of CMC are theoretically analyzed and experimentally verified, which lays theoretical foundation for the EMI suppression in PWM motor system. The rest of this paper is organized as follows, Section II describes the typical topology of PWM motor system, the flowing paths and the mathematical model of CMC. Section III discusses the characteristics of CMC in the aspects of oscillation amplitude/root mean square (rms) value, attenuation time and attenuation period. Experimental results are provided in Section IV to verify the correctness of theoretical analyses. The last part is the conclusion.

II. CMC in PWM Motor System

A. Typical Topology of PWM Motor System

A typical PWM motor system mainly consists of rectifier, inverter and motor, etc. The structure is shown in Fig. 2, where $C_{s1} - C_{s2}$ are the energy storage capacitors. Except distributed capacitance between power cable and ground, there also exist parasitic parameters and distributed capacitances in several other locations of PWM motor system, such as PWM power converter and motor as shown in Fig. 3. The CMV with high changing rate

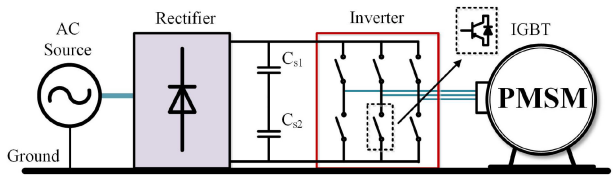

Fig. 2. Typical topology of PWM motor system.

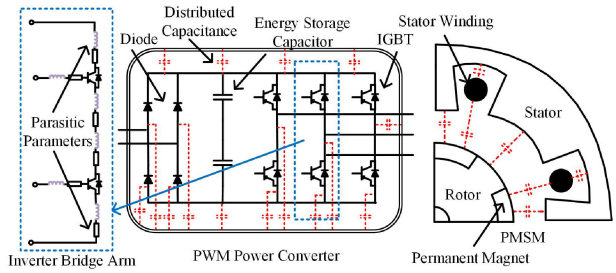

Fig. 3. Parasitic parameters and distributed capacitance in converter and motor.

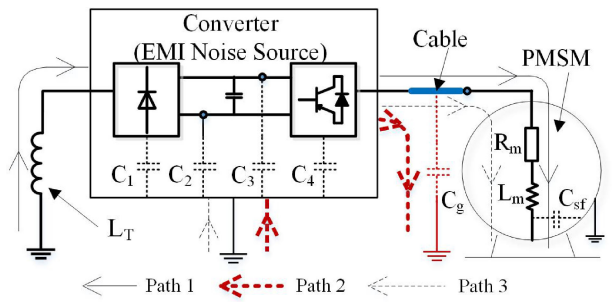

Fig. 4. Diagram of CMC flowing paths.

charges and discharges these distributed capacitances to form CMC.

B. Flowing Paths of CMC

As mentioned above, there are many distributed capacitances in PWM motor system. Thus, these distributed capacitances form multiple closed flowing loops of CMC as shown in Fig. 4, where L_T denotes the inductance of transformer, R_m and L_m denote stator resistance and inductance of PMSM, respectively. C_{sf} denotes distributed capacitance in motor. $C_1 - C_4$ are the distributed capacitances in other locations of PWM motor system, such as the distributed capacitance between power electronic device and converter case, and the distributed capacitance between dc bus and converter case. C_g is the distributed capacitance between cable and ground.

In general, the changing rates of voltage and the values of distributed capacitance are different in different locations of motor system. Hence, the amplitude–frequency characteristics of generated CMC at different positions are also not the same. In addition, because there are multiple flowing paths, the CMC with different amplitude–frequency characteristics are mixed together, which makes it more difficult to measure and analyze CMC. This paper focuses on the research of CMC flowing in path 2 shown in Fig. 4.

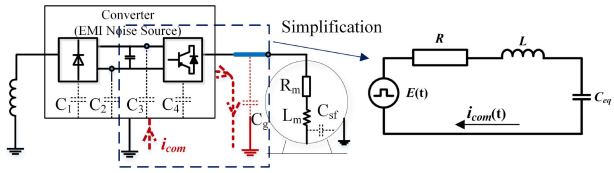

Fig. 5. Simplified CMC flowing path.

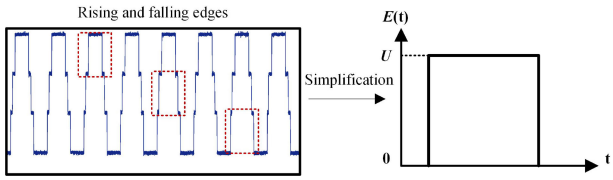

Fig. 6. Simplified CMV waveform.

C. Mathematical Model of CMC

In PWM motor system, the output CMV of inverter is the mean value of three-phase instantaneous voltages and it can be calculated by (1), where $U_{1,2,3}$ are three-phase instantaneous voltages

$$U_{\text{com}} = \frac{U_1 + U_2 + U_3}{3}. \tag{1}$$

According to the principle of equivalent circuit, the flowing path of CMC can be represented as an *RLC* circuit shown in Fig. 5, where *R*, *L*, and C_{eq} are the equivalent resistance, inductance, and capacitance, respectively, *E(t)* denotes the CMV. At the same time, CMC is only generated at the rising and falling edges of CMV, so the CMV waveform can be decomposed into a series of square-wave pulses to facilitate analysis and calculation shown in Fig. 6, where *U* denotes the dc bus voltage.

The CMC can be calculated in accordance with the step response of *RLC* circuit, which can be expressed as an exponentially attenuation waveform as shown in the following:

$$i_{\text{com}}(t) = \frac{U_m}{\sqrt{\frac{L}{C_{eq}} - \frac{R^2}{4}}} e^{-\frac{R}{2L}t} \sin\left(\sqrt{\frac{1}{LC_{eq}} - \frac{R^2}{4L^2}}t\right). \tag{2}$$

In (2), $U_m = +U$ for the rising edge, and $U_m = -U$ for the falling edge. The rms value of CMC is more concerned for the reliability and fault diagnosis of motor system, and the rms value of CMC can be calculated as

$$I_{\text{com}} = \sqrt{\frac{1}{T}\int_0^T i_{\text{com}}^2(t)dt} \tag{3}$$

where *T* is switching cycle. It can be obviously seen from (2) and (3) that the initial oscillation amplitude/rms value, attenuation time, and attenuation period of CMC are mainly related to the following factorsemdashdc bus voltage, equivalent resistance/inductance/capacitance, and the switching frequency of inverter.

The waveform of (2) is simulated using MATLAB/Simulink, where *R* is measured by a multimeter, C_{eq} is determined by the equivalent distributed capacitance artificially added between cable and ground, and *L* is calculated by the measured resonant

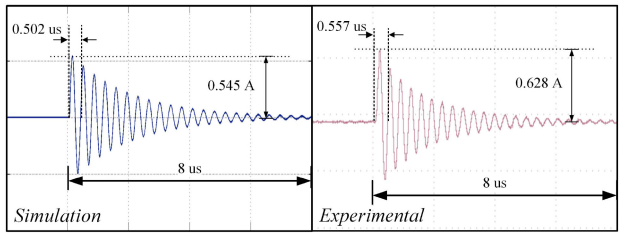

Fig. 7. Simulation and experimental waveforms of CMC.

frequency and C_{eq}. In practical applications, *R*, *L*, and C_{eq} can be measured by impedance analyzer. CMC simulation waveform is compared with experimental waveform under same parameters, the results are shown in Fig. 7. It can be seen from the simulation result in Fig. 7 that the maximum amplitude, attenuation time, and attenuation period of CMC are 0.545 A, 8 μs, and 0.502 μs, respectively, and the CMC waveform ends after 23 attenuation oscillations. For the experimental waveform, the maximum amplitude, attenuation time, and attenuation period of CMC are 0.628 A, 8 μs, and 0.557 μs, respectively, and the CMC waveform also ends after 23 attenuation oscillations. Due to the impacts of system parameters and measuring accuracy, there are some errors between simulation and experimental results, which are within the acceptable range. Therefore, the proposed mathematical model can be used to accurately describe CMC in PWM motor system.

III. Analysis of CMC Characteristics

A. Amplitude/RMS Value of CMC

According to (2), the initial oscillation amplitude of CMC is determined by

$$\text{AMP}_{\text{ini}} = \frac{U_m}{\sqrt{\frac{L}{C_{eq}} - \frac{R^2}{4}}} \tag{4}$$

where AMP_{ini} is the initial oscillation amplitude of CMC. Considering the magnitude of *R*, *L*, and C_{eq} in motor system, according to (3) and (4), there are mainly three factors that affect both the initial oscillation amplitude and rms value of CMC, which include equivalent inductance, equivalent capacitance, and dc bus voltage. In addition, there are two other factors that only affect the rms values of CMC, which are equivalent resistance and switching frequency of inverter.

1) Value of Equivalent Capacitance, Inductance, and Resistance: It can be seen from (4) that AMP_{ini} is positively correlated with U_m and C_{eq}, and negatively correlated with *L*. The impedance of equivalent capacitance and inductance can be expressed as

$$\begin{cases} X_C = \frac{1}{2\pi f C_{eq}} \\ X_L = 2\pi f L \end{cases} \tag{5}$$

where *f* is the frequency of current passing through capacitance or inductance. According to (5), the capacitance impedance is inversely proportional to its own value and the frequency of passed signal, but inductance impedance is proportional to these two

factors. The inductance and capacitance are series connected in CMC flowing path, and the characteristics of CMC are simultaneously affected by the capacitance and inductance. For CMC with specific frequency, the larger the capacitance value, the smaller the equivalent impedance. And the effect of inductance is opposite. For CMC with different frequency, the impedance of capacitance and inductance are also different. And the CMC with resonant frequency can obtain the minimum impedance, which will be detailed analyzed in Part D of this Section.

It can be seen from (4) that the equivalent resistance does not affect the initial oscillation amplitude of CMC, but the resistance can influence the attenuation time of CMC, which may indirectly affect the rms value of CMC. The attenuation time of CMC is detailed analyzed in Part B of this Section.

2) DC Bus Voltage: According to (4) and the voltage–current equation of capacitance shown in (6), the CMC flowing through distributed capacitance is proportional to the changing rate of CMV during each switching operation of power device. In general, the duration of switch ON or OFF of power device can be considered as fixed as several microseconds. So, the CMC passing through distributed capacitance is indirectly related to the value of dc bus voltage

$$i_C = C\frac{du_C}{dt}. \tag{6}$$

For most motor systems, the dc bus voltage is fixed to a constant value which shows little fluctuation during system operation. It is not feasible to reduce dc bus voltage to suppress CMC because low dc bus voltage will deteriorate the drive ability and control performance of motor system. So, some previous researches insert a CM filter in series between the inverter and motor to reduce the changing rate of CMV at motor input side, which can effectively decrease the CMC inside the motor.

3) Switching Frequency of Inverter: In every single switching operation of power device, there is a certain amount of CMC passing through distributed capacitance, and the CMC is an exponentially attenuation waveform as shown in (2) and Fig. 7. So, it is possible to calculate the accurate current amount flowing through distributed capacitance in one switching action. After this, the rms value of CMC in a certain duration is only decided by the switching numbers of power devices which is related to the switching frequency of inverter. Theoretically speaking, the higher the switching frequency, the greater the CMC rms value. For practical applications, the switching frequency of inverter can be properly reduced to suppress CMC while decreasing the switching loss. But it should be noted that low switching frequency will also decrease the control performance of motor system.

B. Attenuation Time of CMC

From the CMC mathematical model in (2) and CMC waveform in Fig. 7, it can be seen that CMC attenuates with time, and the attenuation time is mainly related to the exponential term in (2) as shown in the following:

$$A = e^{-\alpha t}. \tag{7}$$

For the convenience of expression, the attenuation coefficient α is defined as follows:

$$\alpha = \frac{R}{2L}. \tag{8}$$

According to (2), (7), and (8), the attenuation time of CMC changes with the variation of α, and α can be tuned through adjusting the values of *R* and *L*. From (2), it can be seen that the shorter the attenuation time, the smaller the CMC rms value. Thus, CMC can be effectively suppressed by reducing the attenuation time. But the system parameters are generally fixed unless additional devices are artificially added. So, the attenuation time of CMC can be tuned through optimizing system topology or adding filters. It is worth mentioning that, if *R/L* is changed to reduce attenuation time, the initial oscillation amplitude value and attenuation period of CMC will accordingly change, and large resistance consumes more energy. So, it is necessary to determine the R/L value comprehensively in practical applications.

C. Attenuation Period of CMC

It is well known that CMC contains a large amount of high-frequency signals, which are the interference source of PWM motor system. According to the CMC model shown in (2), there is a periodic component P_e in CMC as shown in the following, which is the main source of high-frequency signals.

$$P_e = \sin\left(\sqrt{\frac{1}{LC_{eq}} - \frac{R^2}{4L^2}}t\right). \tag{9}$$

The period T_C of sine function P_e is expressed in the following:

$$T_C = \frac{2\pi}{\sqrt{\frac{1}{LC_{eq}} - \frac{R^2}{4L^2}}}. \tag{10}$$

It can be obviously seen from (9) that T_C changes with the variation of distributed capacitance when *R* and *L* are fixed. The smaller the attenuation period is, the higher the oscillation frequency is. The oscillation can range from a few kHz to several tens of MHz, which may exceed the upper limitation required by EMC standards. Considering the magnitude of *R*, *L*, and C_{eq} in motor system, $R^2/4L^2$ in (10) has little effect on the period T_C and can be ignored. Therefore, the CMC attenuation period can be tuned by adjusting the capacitance and inductance value of equivalent *RLC* flowing path. But it should be noted that the initial oscillation amplitude, rms value, resonant frequency, and other characteristics will also be affected at the same time, which may bring additional harm to motor system.

D. Resonant Frequency of CMC Flowing Loop

In addition to the above-mentioned characteristics, the resonant frequency of CMC flowing loop is also one of the main amplitude–frequency characteristics of CMC. According to the *RLC* circuit as shown in Fig. 5, the resonant frequency of *RLC*

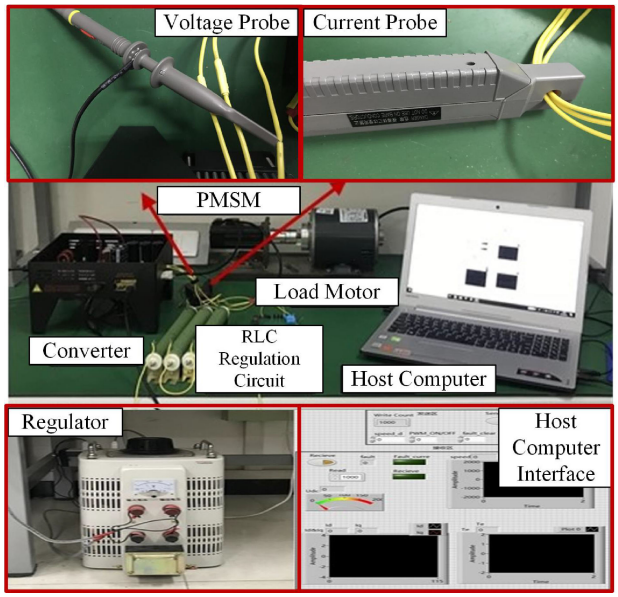

Fig. 8. Test platform setup.

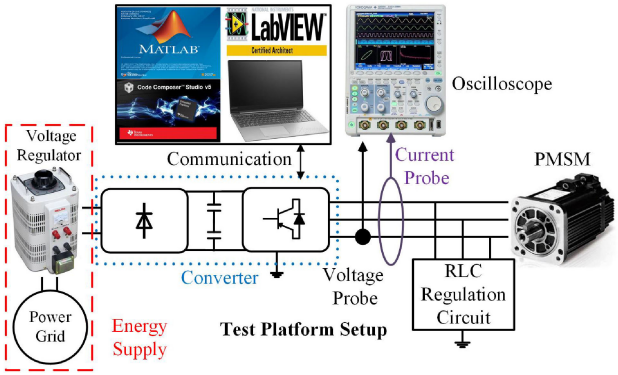

Fig. 9. Schematic diagram of test platform setup.

circuit can be calculated as

$$f_{\text{res}} = \frac{1}{2\pi\sqrt{LC_{eq}}} \tag{11}$$

where f_{res} is series resonant frequency. The components around resonant frequency of CMV are easier to pass through distributed capacitance in motor system, so, the components around resonant frequency accounts for a large proportion of CMC.

If the equivalent resistance and inductance in simplified *RLC* circuit are considered as fixed values, the series resonant frequency shown in (11) is only related to distributed capacitance in motor system. Therefore, the suppression of CMC can be realized through optimizing hardware topology to suppress the CMV/CMC components around series resonant frequency.

IV. Experimental Verification

A. Test Platform Setup

To evaluate the correctness of above theoretical analysis, a PWM motor system test setup has been built as shown in Figs. 8 and 9 is the schematic diagram of test platform setup.

TABLE I
Test Condition and Main Parameters

Parameters	Notation	Value	Unit
Rated power	P_n	0.4	kW
Maximum current	I_{max}	2.8	A
Stator resistance	R_s	2.35	Ω
Stator inductance	L_s	6.5	mH
Rated torque	T_n	1.27	N.m
Pole pairs	n_p	4	-
Switching frequency	f_s	10	kHz
Load	T_L	0	N.m
Test speed	ω_n	1000	r/min
DC bus voltage	U_{dc}	100	V
Capacitance	C_r	250	pF
Resistance	R_r	0	Ω
Inductance	L_r	0	uH

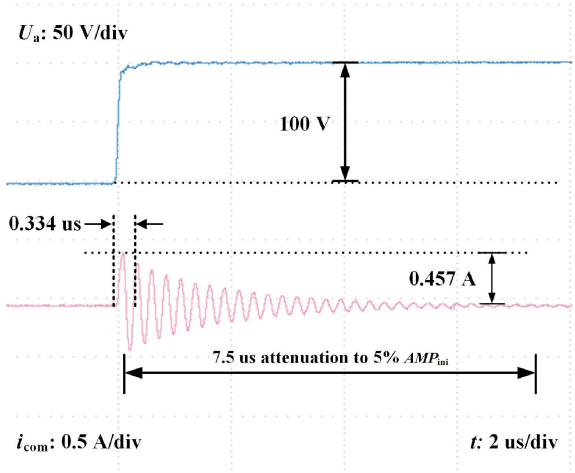

Fig. 10. Motor phase voltage rising edge (upper) and CMC (lower) under 100 V dc bus voltage, 250 pF distributed capacitance, and 10 kHz switching frequency.

A DSP TMS320F28335 controller is utilized to implement field-oriented control strategy and NI LabVIEW is used to build an interaction interface which can modify control parameters and display running status of motor system in real time. The *RLC* regulation circuit can roughly adjust the equivalent capacitance, inductance, and resistance of CMC flowing path through artificially adding capacitor, inductor, and resistor with different values. Especially, the capacitor with different values are added between power cable and ground to simulate distributed capacitance. The test condition and motor parameters are listed in Table I, where capacitance, resistance, and inductance are the parameters of *RLC* regulation circuit.

B. Test Results

In the test process, the motor system operation conditions are remaining unchanged as shown in Table I if there are no special statements. Figs. 10 and 11 are the experimental waveforms of

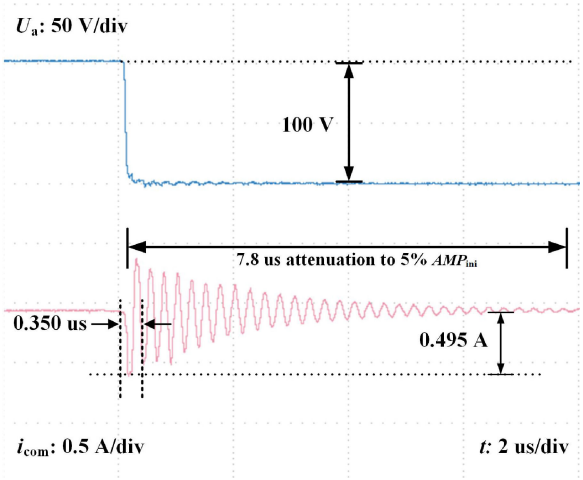

Fig. 11. Motor phase voltage falling edge (upper) and CMC (lower) under 100 V dc bus voltage, 250 pF distributed capacitance, and 10 kHz switching frequency.

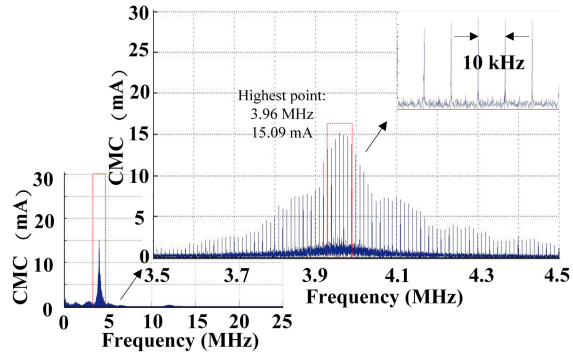

Fig. 12. Frequency spectrum of CMC under 100 V dc bus voltage, 250 pF distributed capacitance, and 10 kHz switching frequency.

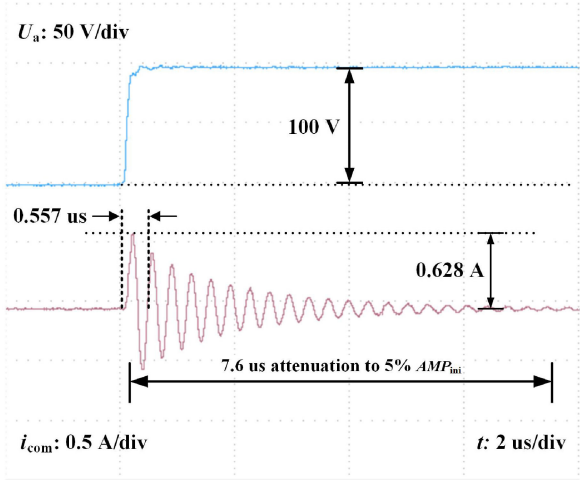

Fig. 13. Motor phase voltage rising edge (upper) and CMC (lower) under 100 V dc bus voltage, 470 pF distributed capacitance, and 10 kHz switching frequency.

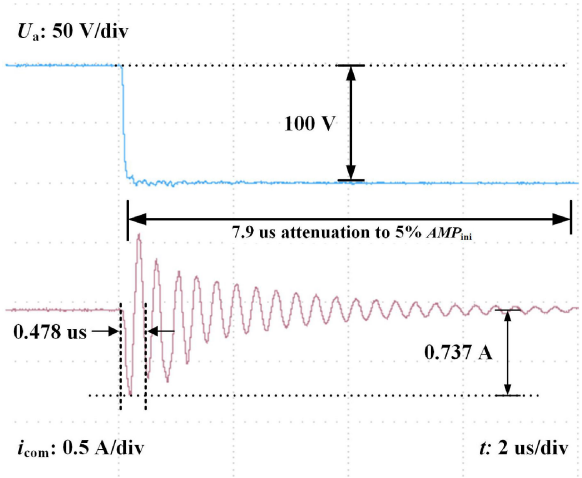

Fig. 14. Motor phase voltage falling edge (upper) and CMC (lower) under 100 V dc bus voltage, 470 pF distributed capacitance, and 10 kHz switching frequency.

motor phase voltage and CMC while the upper waveform is motor phase voltage and the lower waveform is CMC. Fig. 12 is the frequency spectrum of CMC.

It can be obviously seen from Figs. 10 and 11 that, for both rising edge and falling edge of motor phase voltage, the characteristics of CMC, such as initial oscillation amplitude and attenuation time/period, are almost the same, except that the initial oscillation direction is opposite.

According to Fig. 12, the main components of CMC are concentrated around 3.96 MHz which is the resonant frequency, and the frequency interval of main harmonic components is 10 kHz, which is related to the switching frequency of inverter.

Figs. 13 and 14 are the experimental results of motor phase voltage and CMC after increasing distributed capacitance to 470 pF, and the corresponding frequency spectrum of CMC is shown in Fig. 15.

It can be further demonstrated from Figs. 13 and 14 that the rising/falling edge of motor phase voltage has no effect on CMC characteristics except the initial oscillation direction. The initial oscillation amplitude and attenuation period of CMC increase after increasing capacitance value, which is consistent with (5) and (9). But the attenuation time is still about 8 μs because it is not related to capacitance value according to (6). According to the CMC spectrum comparison between Figs. 12 and 15, the resonant frequency of CMC flowing path decreases with the increasing of distributed capacitance, but there is no obvious variation for the maximum value and interval of frequency spectrum.

Since the characteristics of CMC are not affected by the rising/falling state of motor phase voltage, the experimental results during falling state are not given in the following contents. Fig. 16 is the experimental waveforms of motor phase voltage and CMC under 250 pF distributed capacitance, 100 V dc bus voltage and 15 kHz switching frequency, and Fig. 17 is the frequency spectrum of CMC.

It can be found from Figs. 16 and 17 that the characteristics of CMC, such as initial oscillation amplitude and attenuation time/period, show no obvious variation compared with that in Figs. 10 and 12. The only difference is that the interval of frequency spectrum increases to 15 kHz with the increasing of

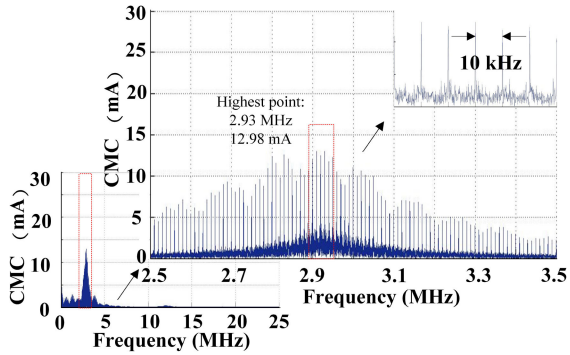

Fig. 15. Frequency spectrum of CMC under 100 V dc bus voltage, 470 pF distributed capacitance, and 10 kHz switching frequency.

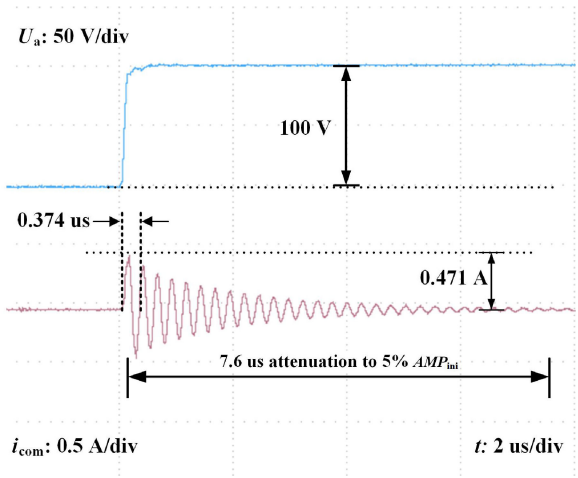

Fig. 16. Motor phase voltage rising edge (upper) and CMC (lower) under 100 V dc bus voltage, 250 pF distributed capacitance, and 15 kHz switching frequency.

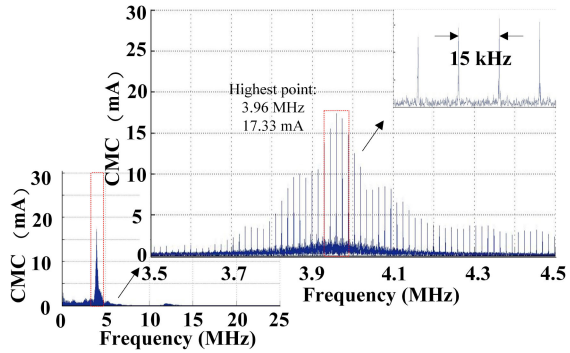

Fig. 17. Frequency spectrum of CMC under 100 V dc bus voltage, 250 pF distributed capacitance, and 15 kHz switching frequency.

inverter switching frequency. Fig. 18 shows the experimental results of CMC under different load and speed.

As shown in Fig. 18, the CMC characteristic variables vary within a small range under different load and speed, which means that the motor speed and load have no obvious effect on CMC. Fig. 19 shows the experimental results of CMC characteristic variables under different equivalent resistance and inductance.

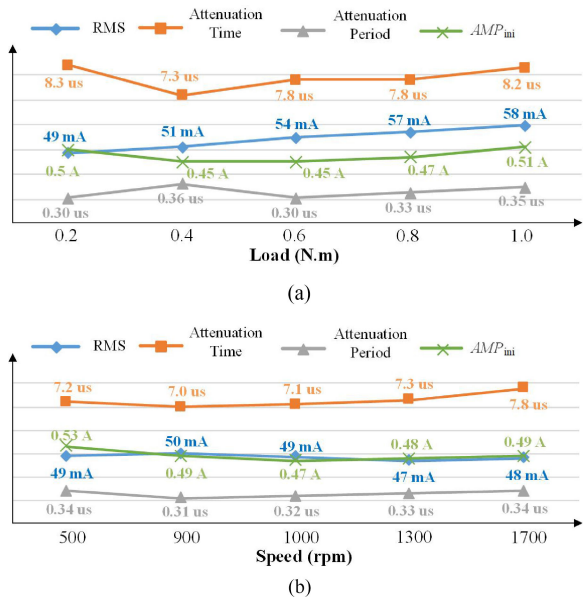

Fig. 18. CMC characteristic variables under different load and speed. (a) CMC characteristic variables under different load. (b) CMC characteristic variables under different speed.

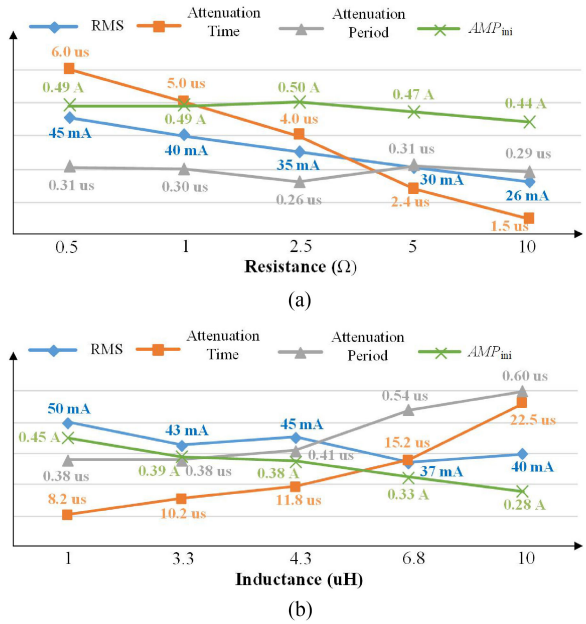

Fig. 19. CMC characteristic variables under different equivalent resistance and inductance. (a) CMC characteristic variables under different equivalent resistance. (b) CMC characteristic variables under different equivalent inductance.

According to Fig. 19(a), the growth of resistance leads to the decrease in rms and attenuation time, while attenuation period and AMP_{ini} remain stable. In Fig. 19(b), the increase of equivalent inductance promotes the increase of attenuation time and attenuation period and the decreases of AMP_{ini}. CMC rms value fluctuates within a small range, which can be considered unaffected. The experimental results in Fig. 19 are consistent with the theoretical analysis in Section III.

Fig. 20 consists of the experimental waveforms of CMC under different values of distributed capacitance, dc bus voltage, and

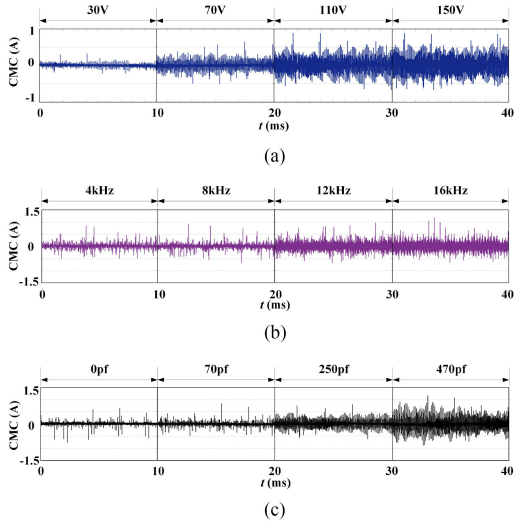

Fig. 20. CMC waveforms under different values of main influencing factors.(a) CMC waveforms under various dc bus voltage. (b) CMC waveforms under various switching frequency. (c) CMC waveforms under various distributed capacitance.

switching frequency. In Fig. 20(a), the dc bus voltage is fixed as 100 V and the switching frequency is fixed as 10 kHz when the distributed capacitance changes. In Fig. 20(b), the switching frequency is fixed as 10 kHz and the distributed capacitance is fixed as 250 pF when the dc bus voltage changes. In Fig. 20(c), the dc bus voltage is fixed as 100 V and the distributed capacitance is fixed as 250 pF when the switching frequency changes.

It can be obviously seen from Fig. 20 that the CMC amplitude and rms value increases in varying degrees with the increasing of distributed capacitance, dc bus voltage, and switching frequency of inverter, which is consistent with the conclusion obtained in part A of Section III.

It can be concluded that the above experimental results are highly consistent with the proposed mathematical model and theoretical analysis, which can effectively verify their correctness.

V. Conclusion

This paper conducts a detailed theoretical analysis and experimental verification for the time–frequency characteristics of CMC. The main conclusions are as follows: The time–frequency characteristics of CMC, include initial oscillation amplitude/rms value, attenuation period/time, and resonant frequency, are mainly affected by motor system parameters, such as dc bus voltage, switching frequency, equivalent resistance/inductance, and distributed capacitance. Specifically, equivalent resistance affects the rms value and attenuation time of CMC, equivalent inductance affects the oscillation amplitude value, attenuation time/period of CMC, distributed capacitance affects the oscillation amplitude/rms value, attenuation period, and resonant frequency of CMC while dc bus voltage only affects the oscillation amplitude/rms value of CMC, and different switching frequency leads to the interval variation of CMC frequency spectrum. The conclusions obtained in this study can provide a theoretical guidance for the effective suppression of CMC.

References

[1] X. Lu, S. Zhang, C. Liu, P. Xie, and H. Chen, "Modeling of common-mode current in motor cable of inverter-fed motor drive system," in *Proc. Asia-Pacific Int. Symp. Electromagn. Compat.*, Shenzhen, China, 2016, pp. 511–514.

[2] P. M. Sunitha, B. Banakara, and S. Reddy, "Modeling, simulation and analysis of common mode voltage, bearing voltage and bearing current in PWM multilevel inverter fed induction motor with long cable," in *Proc. IEEE Int. Conf. Recent Trends Electron. Inf. Commun. Technol.*, Bengaluru, India, 2017, pp. 1161–1167.

[3] X. Pei, "Research of conducted electromagnetic interference in PWM inverter," Ph.D. Dissertation, Huazhong Univ. Sci. Tech., Wuhan, China, 2004.

[4] J. Lai, X. Huang, S. Chen, and T. W. Nehl, "EMI characterization and simulation with parasitic models for a low-voltage high-current ac motor drive," *IEEE Trans. Ind. Appl.*, vol. 40, no. 1, pp. 178–185, Jan./Feb. 2004.

[5] S. Wang, Y. Y. Maillet, F. Wang, R. Lai, F. Luo, and D. Boroyevich, "Parasitic effects of grounding paths on common-mode EMI filters performance in power electronics systems," *IEEE Trans. Ind. Electron.*, vol. 57, no. 9, pp. 3050–3059, Sep. 2010.

[6] E. Gubia, P. Sanchis, A. Ursua, J. Lopez, and L. Marroyo, "Frequency domain model of conducted EMI in electrical drives," *IEEE Power Electron. Lett.*, vol. 3, no. 2, pp. 45–49, Jun. 2005.

[7] S. Ogasawara and H. Akagi, "Modeling and damping of high-frequency leakage currents in PWM inverter-fed ac motor drive systems," *IEEE Trans. Ind. Appl.*, vol. 32, no. 5, pp. 1105–1114, Sep./Oct. 1996.

[8] Z. Shen, D. Jiang, H. Wang, R. Qu, and X. Pei, "Paralleled three-phase four-leg inverters for reduction of common mode current and common mode EMI," in *Proc. Annu. Conf. IEEE Ind. Electron. Soc.*, Beijing, China, 2017, pp. 7028–7033.

[9] Y. Lian, Y. Zhang, Y. Li, N. R. Zargari, and Z. Cheng, "Common-mode resonance suppression in transformerless PWM current-source drive," *IEEE Trans. Power Electron.*, vol. 31, no. 8, pp. 5721–5731, Aug. 2016.

[10] J. Sun and L. Xing, "Parameterization of three-phase electric machine models for EMI simulation," *IEEE Trans. Power Electron.*, vol. 29, no. 1, pp. 36–41, Jan. 2014.

[11] O. Magdun and A. Binder, "High-frequency induction machine modeling for common mode current and bearing voltage calculation," *IEEE Trans. Ind. Appl.*, vol. 50, no. 3, pp. 1780–1790, May/Jun. 2014.

[12] B. Jiang, "Research on the suppression methods of conduction common-mode EMI for PWM motor drive system," *IEEE Trans. Power Electron.*, vol. 31, no. 2, pp. 1408–1424, Feb. 2016.

[13] L. Ran, S. Gokani, J. Clare, K. J. Bradley, and C. Christopoulos, "Conducted electromagnetic emissions in induction motor drive system. II. Frequency domain models," *IEEE Trans. Power Electron.*, vol. 13, no. 4, pp. 768–776, Jul. 1998.

[14] B. Revol, J. Roudet, J. Schanen, and P. Loizelet, "EMI study of three-phase inverter-fed motor drives," *IEEE Trans. Ind. Appl.*, vol. 47, no. 1, pp. 223–231, Jan./Feb. 2011.

[15] D. Han, W. Lee, S. Li, and B. Sarlioglu, "New method for common mode voltage cancellation in motor drives: Concept, realization, and asymmetry influence," *IEEE Trans. Power Electron.*, vol. 33, no. 2, pp. 1188–1201, Feb. 2018.

[16] H. Akagi and R. Kondo, "A transformerless hybrid active filter using a three-level pulse width modulation (PWM) converter for a medium-voltage motor drive," *IEEE Trans. Power Electron.*, vol. 25, no. 6, pp. 1365–1374, Jun. 2010.

[17] C. T. Morris, D. Han, and B. Sarlioglu, "Reduction of common mode voltage and conducted EMI through three-phase inverter topology," *IEEE Trans. Power Electron.*, vol. 32, no. 3, pp. 1720–1724, Mar. 2017.

[18] N. Mutoh and M. Ogata, "New methods to control EMI noises generated in motor drive systems," *IEEE Trans. Ind. Appl.*, vol. 40, no. 1, pp. 143–152, Jan./Feb. 2004.

[19] H. Akagi and T. Shimizu, "Attenuation of conducted EMI emissions from an inverter-driven motor," *IEEE Trans. Power Electron.*, vol. 23, no. 1, pp. 282–290, Jan. 2008.

[20] M. C. Cavalcanti, K. C. de Oliveira, A. M. de Farias, F. A. S. Neves, G. M. S. Azevedo, and F. C. Camboim, "Modulation techniques to eliminate leakage currents in transformerless three-phase photovoltaic systems," *IEEE Trans. Ind. Electron.*, vol. 57, no. 4, pp. 1360–1368, Apr. 2010.

[21] N. Bondarenko *et al.*, "A measurement-based model of the electromagnetic emissions from a power inverter," *IEEE Trans. Power Electron.*, vol. 30, no. 10, pp. 5522–5531, Oct. 2015.

Shiran Cao was born in Hunan, China, in 1993. He received the B.S. degree in electrical engineering from Changsha University of Science and Technology, Changsha, China, in 2015. He is currently working toward the M.S. degree in electrical engineering at the Hebei University of Technology, Tianjin, China.

His main research interests include power electronics and electromagnetic compatibility for motor drive applications.

Feng Niu (M'15) was born in Hebei, China, in 1986. He received the B.S and Ph.D. degrees from the Hebei University of Technology, Tianjin, China, in 2009 and 2015, respectively, both in electrical engineering.

He is currently an Associate Professor with the School of Electrical Engineering, Hebei University of Technology. From September 2012 to September 2014, he was a Research Fellow with the Electrical Machines and Drives Laboratory, Michigan State University, East Lansing, MI, USA. He has authored and coauthored more than 30 technical articles. His research interests include motor system and control, power converter control, and intelligent electrical equipment.

Xiaoyan Huang (M'09) received the B.E. degree in control measurement techniques and instrumentation from Zhejiang University, Hangzhou, China, in 2003, and received the Ph.D. degree in electrical machines and drives from the University of Nottingham, Nottingham, U.K., in 2008.

From 2008 to 2009, she was a Research Fellow with the University of Nottingham. She is currently a Professor with the College of Electrical Engineering, Zhejiang University, Hangzhou, China, where she is working on electrical machines and drives. Her research interests include PM machines and drives for aerospace and traction applications, and generator systems for urban networks.

Shaopo Huang was born in Hebei, China, in 1986. He received the B.S. and M.S. degrees in electrical engineering from the Hebei University of Technology, Tianjin, China, in 2009 and 2015, respectively, where he is currently pursuing the Ph.D. degree in electrical engineering.

Since 2016, he has been a Research Fellow with the Electrical Machines and Drives Laboratory, Michigan State University, East Lansing, MI, USA. His current research interests include reliability and life prediction of electrical apparatus and fault diagnosis of motors.

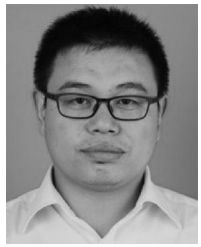

Yao Wang (M'16) was born in Hebei, China, in 1981. He received the B.S., M.S., and Ph.D. degrees from the Hebei University of Technology, Tianjin, China, in 2006, 2009, and 2012, respectively, all in electrical engineering.

He is currently an Associate Professor with the School of Electrical Engineering, Hebei University of Technology. He has authored and coauthored more than 20 technical articles. His research interests include intellectualization of electrical apparatus and fault detection and mitigation for microgrids.

Kui Li was born in Hebei, China, in 1965. He received the B.S. and M.S. degrees from the Hebei University of Technology, Tianjin, China, in 1987 and 1992, respectively, and the Ph.D. degree from Fuzhou University, Fuzhou, China, in 1996, all in electrical engineering.

He is currently a Professor with the School of Electrical Engineering, Hebei University of Technology. He has coauthored more than 100 technical articles and two monographs. His research interests include reliability and intellectualization of electrical apparatus, fault diagnosis, and life prediction of electrical apparatus.

Youtong Fang (M'11–SM'15) received the B.S. and Ph.D. degrees in electrical engineering from the Hebei University of Technology, Hebei, China, in 1984 and 2001, respectively.

He is currently a Professor with the College of Electrical Engineering, Zhejiang University, Hangzhou, China. His research interests include the application, control, and design of electrical machines.